Stability of the Thermohaline Circulation to Noisy Surface Buoyancy Forcing for the Present and a Warm Climate in an Ocean General Circulation Model

ØYSTEIN SKAGSETH AND KJELL ARNE MORK

Geophysical Institute, University of Bergen, Bergen, Norway

(Manuscript received 6 August 1996, in final form 6 August 1997)

ABSTRACT

The stabilities of two different circulation regimes in the North Atlantic, 1) the present thermohaline circulation and 2) a weaker thermohaline circulation, are compared using the Hamburg Large Scale Geostrophic (LSG) ocean circulation model. The latter circulation regime is obtained by restoring the LSG model toward an on average 4°C warmer air surface temperature corresponding to a doubled atmospheric content of CO_2. The stabilities of these stationary states are investigated by imposing various amounts of stochastic noise on the surface freshwater flux.

The simulations show more variability on secular timescales for the present than for the warm climate. Since the modeled static stabilities for the two climates are relatively similar, the different rates of variability are probably connected to other mechanisms. In the present climate at high latitudes the two buoyancy fluxes due to heat and freshwater are of similar magnitudes but with opposite signs; thus switches between convective and nonconvective periods at secular timescales are possible. In the warm climate the buoyancy flux due to heat dominates. This compensates the effect of the noisy freshwater forcing and thus reduces the potential for secular oscillations. The stronger coupling between the Atlantic and the Southern Ocean for the present relative to the warm climate could also contribute to this difference.

Furthermore, the simulations show that the variability of the Antarctic Circumpolar Current transport for the present climate exceeds that of the warm climate. For increasing stochastic noise the present circulation approaches that of the warm circulation.

The authors apply a mixture of heat flux and temperature restoring for the surface boundary condition. Comparison with similar works, which apply a pure restoring for surface temperature, shows that the ocean circulation is much less sensitive to forced stochastic freshwater anomalies with the type of boundary condition used herein. A box model is used to illustrate the effects of the surface temperature parameterizations and the different buoyancy forcing for the present and warm climate.

1. Introduction

On timescales of tens to hundreds of years, the ocean absorbs atmospheric fluctuations (Hasselmann 1976) thereby buffering rapid climate changes in the atmosphere. However, there is also mounting evidence that the ocean itself has several distinct modes of circulation. Paleoclimate research shows that the North Atlantic Deep Water (NADW) formation varied drastically during glacial times (Boyle and Keigwin 1987; Broecker 1991; Keigwin et al. 1991). Results from the GISP-2 ice core indicate switches between glacial and near-interglacial states during the Pleistocene in periods of less than a decade (Taylor et al. 1993). The variability during glacial periods is potentially connected to rapid ice cap melting. During interglacials, changes in the haline forcing are due to changes in the precipitation and evaporation fields. These changes are associated with long timescales and small amplitudes. This could explain the relatively small climatic variability during the present interglacial (Boyle and Keigwin 1987).

The thermohaline circulation has been studied with various simplified models. Stommel (1961) was the first to note that, by applying different restoring times for the salinity and temperature surface conditions, multiple distinct stable circulation regimes are possible. Bryan (1986) used an idealized sector model to investigate the stability of the thermohaline circulation due to surface salinity anomalies. He found that the symmetric equatorial circulation regime was unstable in contrast to the asymmetric state, which was stable. Marotzke et al. (1988) found similar results with a zonally averaged meridional-plane model.

The variability of different ocean circulation regimes has been addressed in several ocean general circulation model (OGCM) simulations that include realistic topography. Toggweiler and Samuels (1993) concluded that oscillations were favored in the case of a weak North Atlantic overturning based on simulations with the Geophysical Fluid Dynamics Laboratory (GFDL)

Corresponding author address: Dr. Oystein Skagseth, Geophysical Institute, University of Bergen, Allegt. 70, 5007 Bergen, Norway.
E-mail: skagseth@gfi.uib.no

OGCM with altered zonal wind stress in the ACC. In contrast, results of simulations with the Hamburg Large Scale Geostrophic (LSG) OGCM showed that oscillations are more pronounced for the case of a strong North Atlantic overturning (Pierce et al. 1995; Mork and Skagseth 1996).

Thermohaline oscillations may evolve if the buoyancy fluxes due to the heat forcing and freshwater forcing are of comparable magnitude. Welander (1986) gives examples of simple heat–salt oscillators that illustrate this effect. The sensitivity of the ocean to surface freshening at high latitudes is demonstrated in several OGCM simulations (e.g., Bryan 1986; Marotzke 1989; Maier-Reimer and Mikolajewicz 1989). Maier-Reimer and Mikolajewicz (1989) showed that only a small amount of meltwater, 0.011 Sv (Sv $\equiv 10^6\ m^3\ s^{-1}$), from the St. Lawrence River was needed to collapse the Atlantic thermohaline circulation in the LSG model. This is referred to as the ''polar halocline catastrophe'' (Bryan 1986).

Recently, several OGCM simulations have been performed by superimposing stochastic noise on the freshwater flux to investigate the stability and variability of the thermohaline circulation (e.g., Mikolajewicz and Maier-Reimer 1990; Mysak et al. 1993; Weaver et al. 1993; Barnett et al. 1993; Power 1995; Pierce et al. 1995). In a simulation with the Hamburg LSG model Mikolajewicz and Maier-Reimer (1990) achieved large thermohaline oscillations with a period of 320 yr when white noise with a standard deviation of 16 mm/month was added to the freshwater fluxes. Pierce et al. (1995), using the same model, showed that similar oscillations also develop when the freshwater flux is uniformly reduced by 7.5% or increased by 10%. The oscillations originated in the Southern Ocean and the generating mechanism was switches in the leading terms in the buoyancy forcing between the stabilizing freshwater flux and the destabilizing heat flux due to nonlinearities in the equation of state. In the state with reduced thermohaline circulation a freshwater cap developed (due to the positive net freshwater flux), which prevented the water column from overturning. During this period, heat transported by advection and diffusion from the North Atlantic Deep Water to the Southern Ocean accumulated in the subsurface layers ($\sim$300 m) until the water column became unstable and overturned. The heat then vented to the atmosphere, which again reduced the convection rate and the cycle repeated. Thermohaline oscillations caused by subsurface heating are also found in another OGCM (Winton and Sarachik 1993).

Power (1995) added white noise to the freshwater flux under both restoring and mixed boundary conditions to study the drift of the equilibrium state of the GFDL modular ocean model. The noise had a standard deviation of 54 mm/month and was added globally, equatorially, or at high latitudes. In contrast to Mikolajewicz and Maier-Reimer (1990), the model generated no secular oscillations. Since the LSG and GFDL models have different transports across the Antarctic Circumpolar Current (ACC), their potentials for generating secular oscillations are different (Pierce et al. 1995). Significant drift in the strength of the ACC was only seen when the noise was added to the freshwater flux at high latitudes under mixed boundary conditions. In simulations with noise added to the heat flux, Power (1995) found no drift or oscillations in the ACC.

Several authors (Rahmstorf and Willebrand 1995; Power and Kleeman 1994; Power 1995; Mikolajewicz and Maier-Reimer 1994) have shown that the parameterization of the surface heat flux is essential in studying the variability and the stability of the thermohaline circulation. Under mixed boundary conditions there is a strong restoring between the ocean and the atmosphere that makes the thermohaline circulation in OGCMs sensitive to climatic fluctuations, while more realistic boundary conditions seem to stabilize the thermohaline circulation. Mikolajewicz and Maier-Reimer (1994) demonstrated that using a mixture of weaker restoring and prescribed flux in the heat flux parameterization increases the stability of the thermohaline circulation.

This study aims at comparing the stability of two different North Atlantic circulation regimes: 1) the present thermohaline circulation and 2) a weaker thermohaline circulation to noisy surface buoyancy forcing. The latter circulation regime is obtained by restoring the Hamburg LSG model toward surface temperature corresponding to a doubled atmospheric content of CO_2 while the wind stress and freshwater flux forcing are similar to those of the present climate. The stability of these stationary states is investigated by imposing various amounts of stochastic noise on the freshwater flux. The relative effects of the stochastic noise on the buoyancy fluxes are different for these two states due to nonlinear terms in the equation of state. We will relate this to the results of the simulations with the LSG model. Furthermore, the parameterization of the surface heat flux is discussed. A box model is used to illustrate the effects of the sea surface temperature (SST) parameterizations and the different buoyancy forcing for the two climates. Finally, we address the question of whether the extent of oscillations depends on the strength of the North Atlantic overturning.

2. The model

For the simulations we used the Hamburg LSG OGCM (Maier-Reimer et al. 1993). The architecture of this model is based on Hasselmann's (1982) suggestion that for large-scale ocean circulation models designed for climate studies, the relevant timescale is much longer than the timescale for gravity and barotropic Rossby wave modes, whereas the relevant spatial scales are large compared with the internal Rossby radius. Thus, it neglects the advection of momentum in the primitive equations. The model is based on the conservation of salt, heat, and momentum; the full equation of state; and

the hydrostatic approximation. The LSG model includes a thermodynamic sea ice model where sea ice is advected with the surface currents. Convective adjustment is performed by interchanging water masses between the layers whenever the water column becomes unstable. Model numerics are implicit and unconditionally stable. Its time step is 30 days, a compromise between the need to resolve the annual cycle versus the potential to take longer time steps because of the LSG formulation. The model has a realistic topography with an effective horizontal resolution of 3.5° × 3.5°. Vertically, it is resolved by 11 layers (specified at depths of 25, 75, 150, 250, 450, 700, 1000, 2000, 3000, 4000, and 5000 m).

Surface boundary conditions are provided by the monthly mean wind-stress climatology of Hellerman and Rosenstein (1983), the monthly mean air temperature from the Comprehensive Ocean–Atmosphere Data Set (COADS) (Woodruff et al. 1987), and the annual mean surface salinity from Levitus (1982) (the annual mean was preferred to the seasonal dataset due to the sparseness of the data). The SST is restored toward an effective air surface temperature, which is retrieved by combining the COADS dataset with the surface winds in an advection equation (Maier-Reimer et al. 1993). The motivation for this is that the climatological mean values are unable to capture the strong heat transfer to the atmosphere through subtimescale processes. In the initialization run, restoring conditions are used for SST and surface salinity with a restoring time constant of respectively 60 and 40 days.

The initial conditions were homogeneous, a water mass having a potential temperature of 2.5°C and a salinity of 34.5 psu. After 10 000 years of integration, the model was nearly at equilibrium with a residual trend of less than 2×10^{-6} °C/yr and 5×10^{-8} psu/yr at 4000-m depth. Diagnostic freshwater fluxes required to restore the surface salinity to climatological values were calculated from the salinity boundary condition during the last 500 years of the spinup. The model was then run for another 4000 years using diagnostic freshwater fluxes until it reached a new stable situation (similar to that after 10 000 years).

After the spinup of the model with the diagnosed freshwater fluxes, the heat flux parameterization was changed to a parameterization suggested by Mikolajewicz and Maier-Reimer (1994). They argued that a pure restoring condition damps out SST anomalies too rapidly. Instead they introduced a mixture of prescribed heat flux and weaker temperature restoring for the surface temperature condition

$$\frac{dT}{dt} = \frac{H_{fc}}{\Delta z \rho c_p} + \frac{(T_c - T)}{\tau}. \quad (1)$$

The heat flux (H_{fc}) needed to maintain the stationary circulation defined by the control run is

$$H_{fc} = \kappa(T_a - T_c), \quad (2)$$

where T_c is the ocean model climate for the control run and κ is the coupling coefficient. The heat flux for the present climate was diagnosed from the last 500 years of the run with diagnostic freshwater fluxes, whereas the heat flux for the warm climate was diagnosed from the last 500 years of a run where the SST was restored toward a $2 \times CO_2$ climate.

Frankignoul and Hasselmann (1977) reported a typical lifetime of SST anomalies in the North Pacific of 6 months, which is significantly longer than the 2 months based on the Newtonian coupling formulation. This is based on local air–sea transfer experiments (Mikolajewicz and Maier-Reimer 1994) and is equivalent to an air–ocean heat exchange coefficient of 40 W m^{-2} K^{-1} for an ocean mixed layer thickness of 50 m. Mikolajewicz and Maier-Reimer (1994) showed that a choice of κ of 27–16 W m^{-2} K^{-1} gave reasonable results for the sensitivity of the NADW formation, and that both transition from ON to OFF mode and the reverse are possible for this choice. Seager et al. (1995) used an atmospheric mixed layer model in SST anomalies simulations to show that the relaxation coefficient κ could at the most reach about 15 W m^{-2} K^{-1}. For the simulations where stochastic noise is superimposed on the freshwater flux we chose 16 W m^{-2} K^{-1} for κ, which is equivalent to a restoring time (τ) of 5 months. Nevertheless, since the modeled thermohaline variability is sensitive to the surface heat boundary condition, only the qualitative aspects of the results presented in the following sections are likely to be meaningful, whereas the quantitative details are probably unrealistic.

As examples of how the model is able to reproduce the gross features of the present climate, zonally averaged meridional fields of potential temperature, salinity, and potential density (sigma-theta) from the control run are compared with observations (Levitus and Boyer 1994; Levitus et al. 1994). The modeled and the observed values of potential temperature (Fig. 1) and salinity (Fig. 2) are relatively similar in the upper ocean. For temperature this is not surprising since a restoring condition is used for the surface layer [Eq. (1)]. This is also the case for salinity although a pure flux condition for freshwater is applied. However, this is due to the similar circulation regime when the flux condition is used to that when the salinity restoring was used. For the intermediate and deep ocean the main distribution is similar for the observed and modeled fields, but for the control run the ocean is warmer and saltier compared to the observed fields. The most pronounced difference in salinity is seen in the Southern Ocean. Figure 3 shows that the model field for potential density does not differ significantly from the observed values. Hence the individual errors of temperature and salinity in the model tend to cancel each other out in terms of density.

3. Description of the experiments

A schematic view of the simulations is shown in Fig. 4. The stochastic freshwater flux simulations are divided

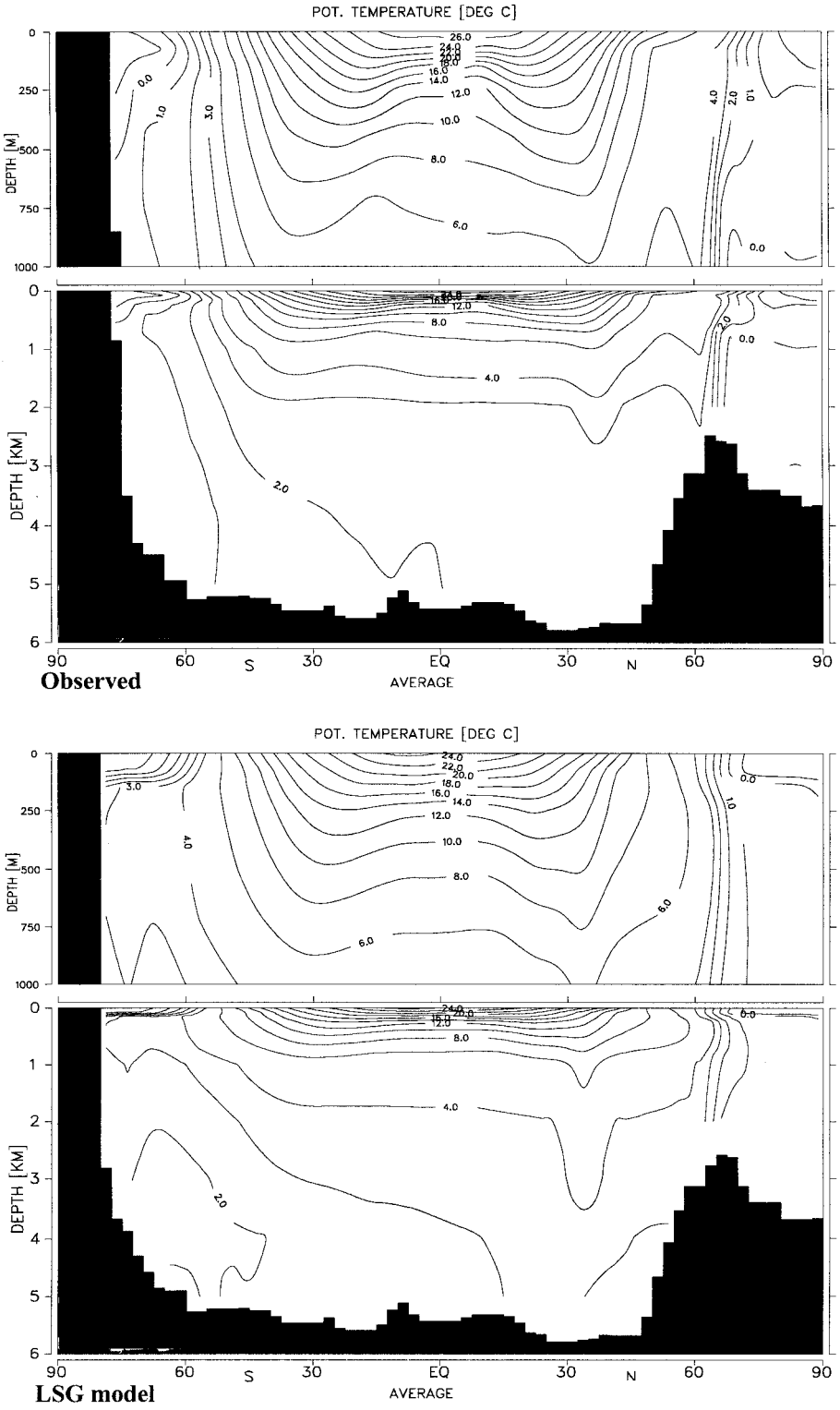

FIG. 1. Annual global zonal average of temperature from (a: top panel) Levitus and Boyer (1994) dataset and (b: bottom panel) the control run of the LSG model.

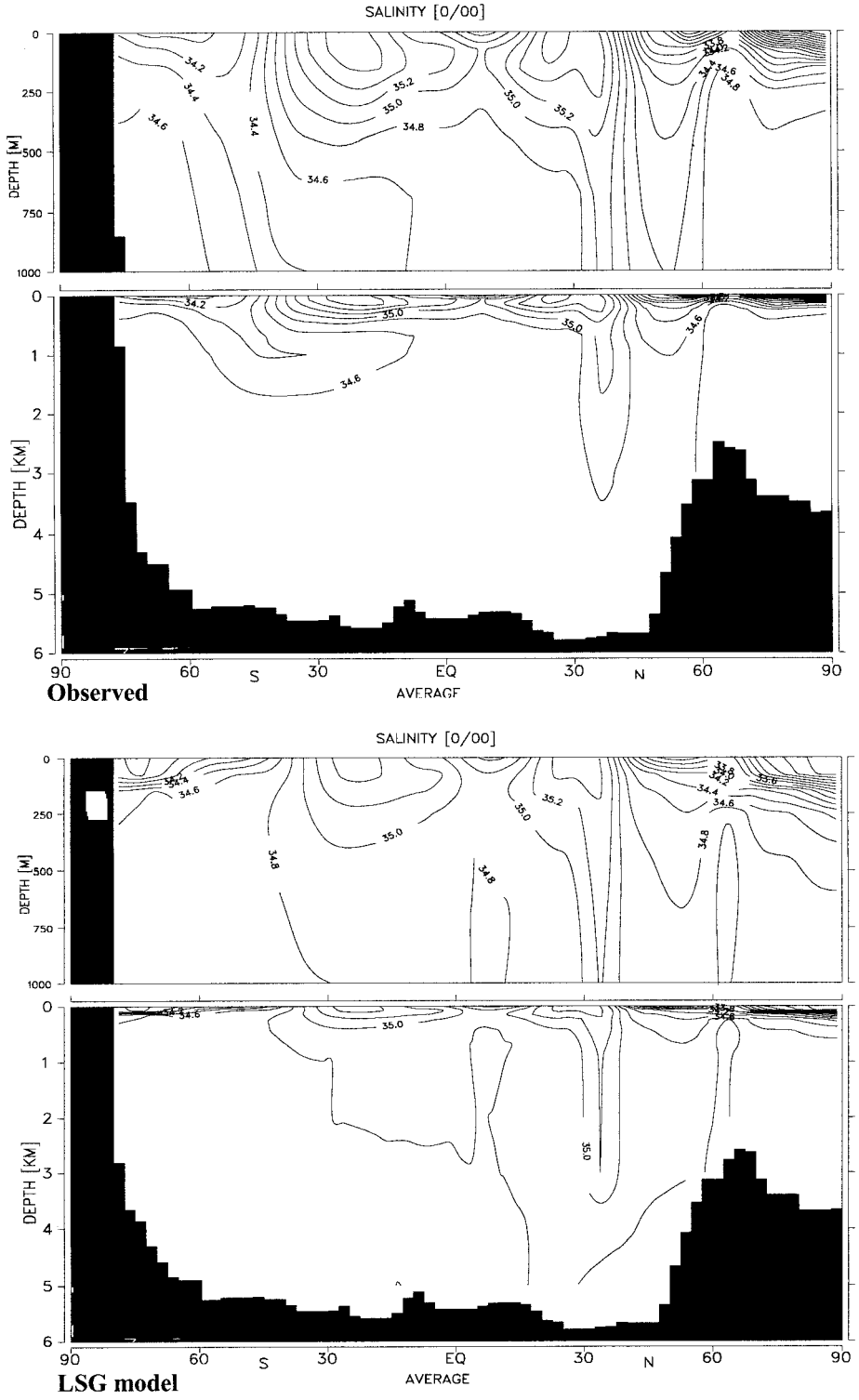

FIG. 2. Annual global zonal average of salinity from (a: top panel) Levitus et al. (1994) dataset and (b: bottom panel) the control run of the LSG model.

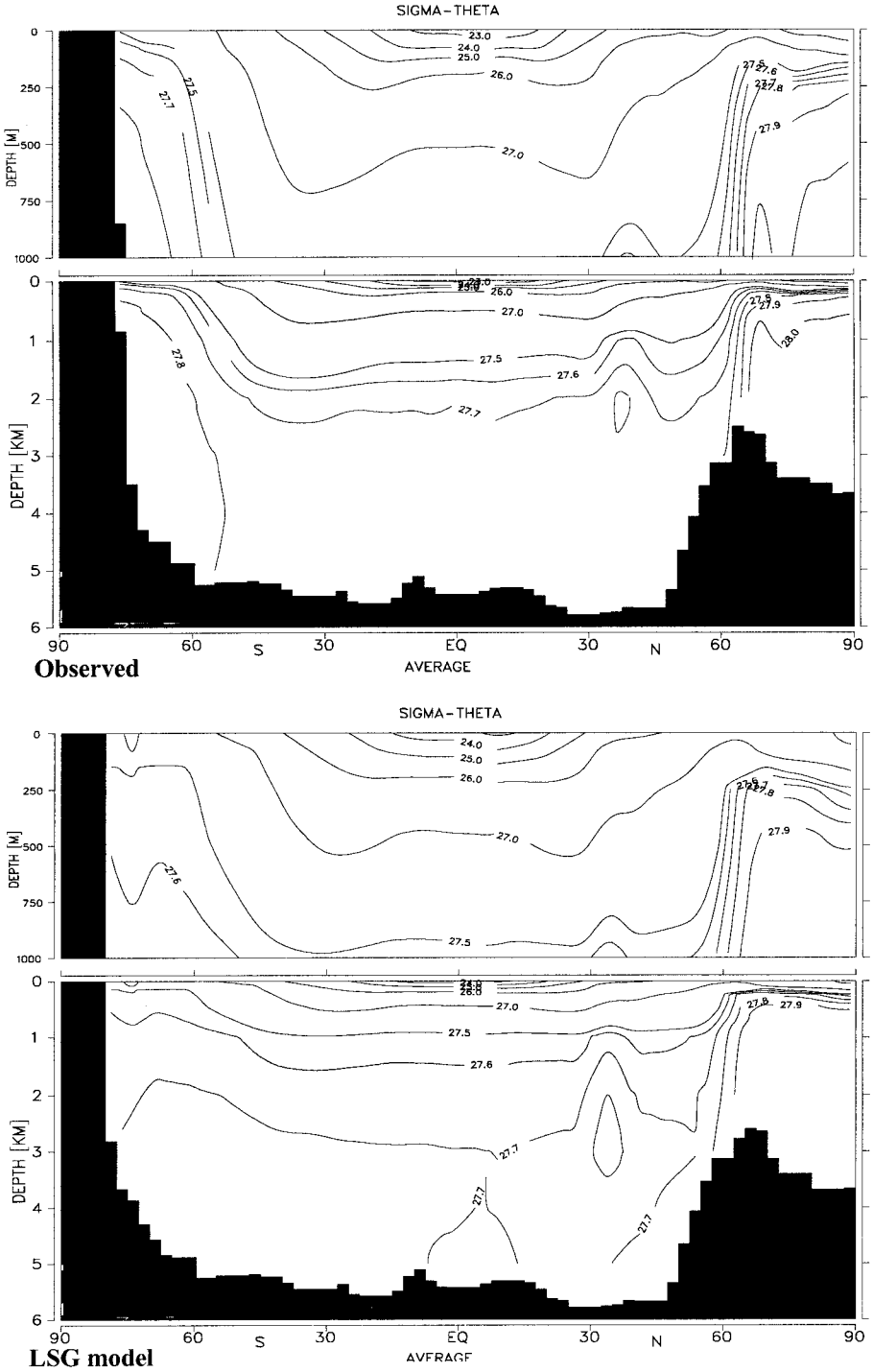

FIG. 3. Annual global zonal average of σ_θ from (a: top panel) observations and (b: lower panel) the control run of the LSG model.

into two parts. One part originates from an equilibrium ocean state for the present climate while the other part starts from a state corresponding to a $2 \times CO_2$ climate, which has a weaker North Atlantic thermohaline circulation (meridional circulation plots are shown later). After the model spinup with the diagnostic freshwater fluxes toward the state that corresponds to the present climate, a new spinup (2000-yr run) is done toward a warmer climate. The SST is restored to a surface air temperature corresponding to a $2 \times CO_2$ climate. The

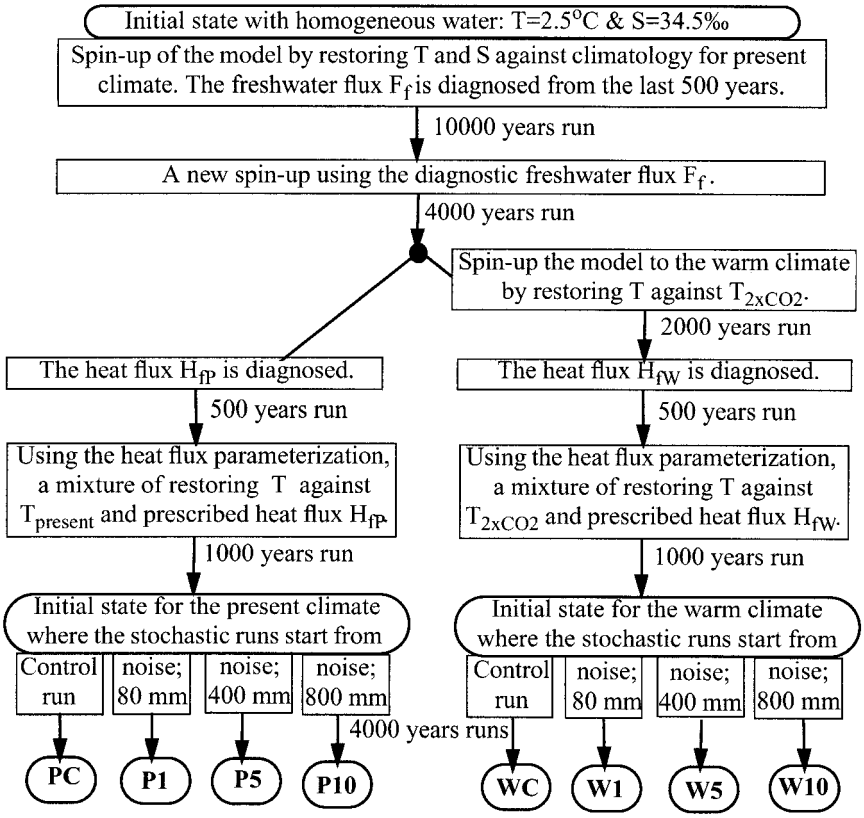

FIG. 4. A schematic view of the stochastic simulations. **PC**, **P1**, . . . , **W10** is the name of each simulation. The number after **P** (present climate) or **W** (warm climate) indicates the magnitude of the noise; **1** is a simulation where noise is added to the freshwater fluxes with a standard deviation of 80 mm/month while the number **5** or **10** is respectively a five or ten fold increase of the noise relative to that simulation. **C** stands for control run (no noise).

surface air temperature field is an average of four equilibrium response simulations with different AGCMs simulating a doubling of CO_2 (Hansen et al. 1984; Schlesinger and Zhao 1989; Wetherald and Manabe 1986; Wilson and Mitchell 1987). The anomaly fields are positive everywhere and the global mean warming over the oceans is 4°C (Fig. 5).

Under this spinup the other boundary fields are unchanged. From these two equilibrium states, which correspond to the present and the warm climate, the heat fluxes are diagnosed, averaged over a 500-yr run (Fig. 6). At low latitudes there are minor differences between the fluxes, while at high latitudes there are significant differences. Especially in convective areas (Southern Ocean and Nordic Seas) there is increased heat loss from the ocean to the atmosphere for the warm climate relative to the present climate. Most of these changes are due to a reduced ice cover (not shown). The model was integrated another 1000 years for both climates using the heat flux parameterization suggested by Mikolajewicz and Maier-Reimer (1994) (mixture of temperature restoring and prescribed heat flux). These runs are done to make sure the model is still in an equilibrium state for the two climates. From these two states the stochastic simulations start.

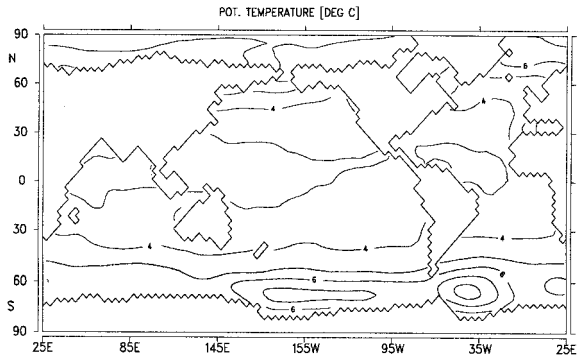

FIG. 5. The annual mean surface air temperature anomaly (2 × CO_2 − present). The contour interval is 1°C.

Four stochastic simulations are performed for each climate where white noise with different amplitudes is added to the freshwater fluxes. The chosen standard deviation of the noise is: 0 (the control run), 80 mm/month, 400 mm/month, and 800 mm/month. The 80 mm/month is equal to the globally averaged annual mean precipitation (Baumgartner and Reichel 1975).

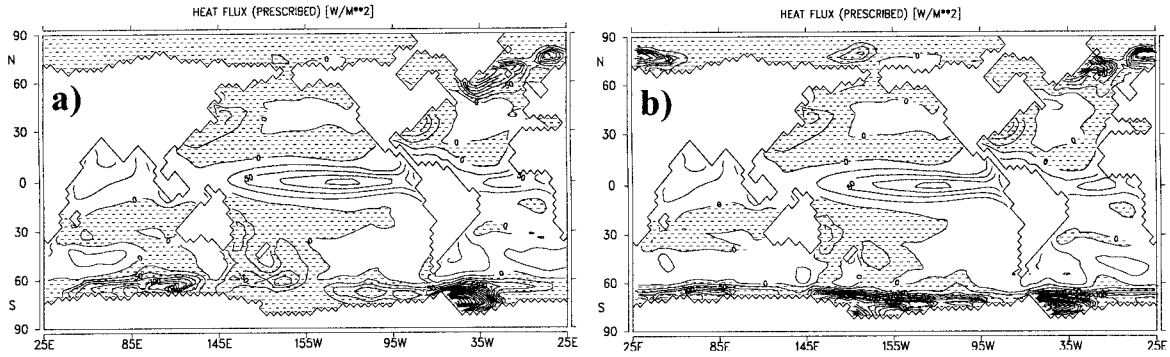

FIG. 6. The prescribed heat fluxes used in the heat flux parameterization: (a) the present climate (H_{fp}); (b) the warm climate (H_{fw}). The figures show annual means. Negative values (heat loss from the ocean to the atmosphere) are shaded.

The stochastic component S, which is added to the freshwater flux, is represented as a sum of Fourier components

$$S(x, y) = A\left[\sum_k \cos(kx + \varphi_k) + \sum_l \cos(ly + \varphi_l)\right], \quad (3)$$

where k and l are the wavenumbers in the x and y directions respectively, φ_k is a random phase but constant for each k and y (independent of x and l), and φ_l has a similar form to φ_k but is constant for l and x. The amplitude A is the same for all wavenumbers (white noise). The wavenumbers k and l are respectively given by

$$k \in \frac{2\pi}{N\Delta x}, \frac{4\pi}{N\Delta x}, \frac{6\pi}{N\Delta x}, \ldots, \frac{\pi}{\Delta x}$$

$$l \in \frac{2\pi}{M\Delta y}, \frac{4\pi}{M\Delta y}, \frac{6\pi}{M\Delta y}, \ldots, \frac{\pi}{\Delta y},$$

where N and M are the number of grid points in x and y directions; Δx and Δy are the model grid sizes. Since the formulation of the random forcing field is based on Cartesian coordinates and the ocean model is based on spherical coordinates, the area mean of the stochastic forcing fields may differ from zero. This difference is small but, to assure that no trend in the average salinity occurs, the global mean of the random forcing fields (based on spherical coordinates) is removed at every time step. The amplitude A is computed to give the desired standard deviation using only wet points in the model.

Ideally, a new stochastic forcing field should be generated for each time step. However, for computational reasons we generated a priori 100 stochastic fields from which we chose randomly. In all simulations, the same sequence of stochastic fields was used.

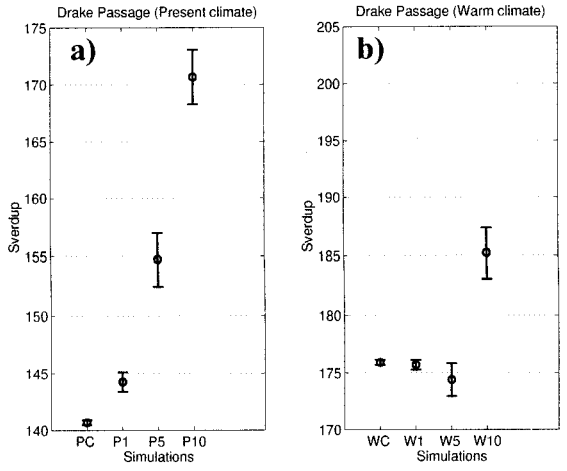

FIG. 7. Values of the mean volume transport through Drake Passage with different amplitudes of the freshwater noise for (a) the present climate and (b) the warm climate. The bars show the standard deviation. The last 2000 years of the simulations (year 2000–4000) are used to calculate the means and the standard deviations of the transports.

4. Results

We discuss the results in terms of transport through Drake Passage for several reasons. It reflects the rate of deep-water formation in the Southern Ocean. Weaker deep-water formation reduces the north–south density gradient, thereby reducing the geostrophic velocities in the ACC. Furthermore it has been focused on in other OGCM simulations, which makes comparison easier. Figure 7 shows the mean transport through Drake Passage over the last 2000 years of the simulations. The transports for the control runs PC and WC are respectively 141 Sv and 176 Sv. The drift, hereof defined as the rate of change in ACC with increasing noise, is much larger for the present climate (Fig. 7a) than for the warm climate (Fig. 7b); for example, the transport increases about 14 Sv for P5 and 1 Sv for W5. For the present climate with high noise (P10), the ACC transport approaches that of the warm climate. The standard deviations of the transports (shown as bars) for P1 and P5 are respectively 1 and 2.5 Sv compared to 0.5 and 1.4 Sv for W1 and W5. For P10 and W10 the standard deviations are similar for both climates (about 2.5 Sv). The general trend is increased variability for increased noise in the freshwater forcing. However, the results

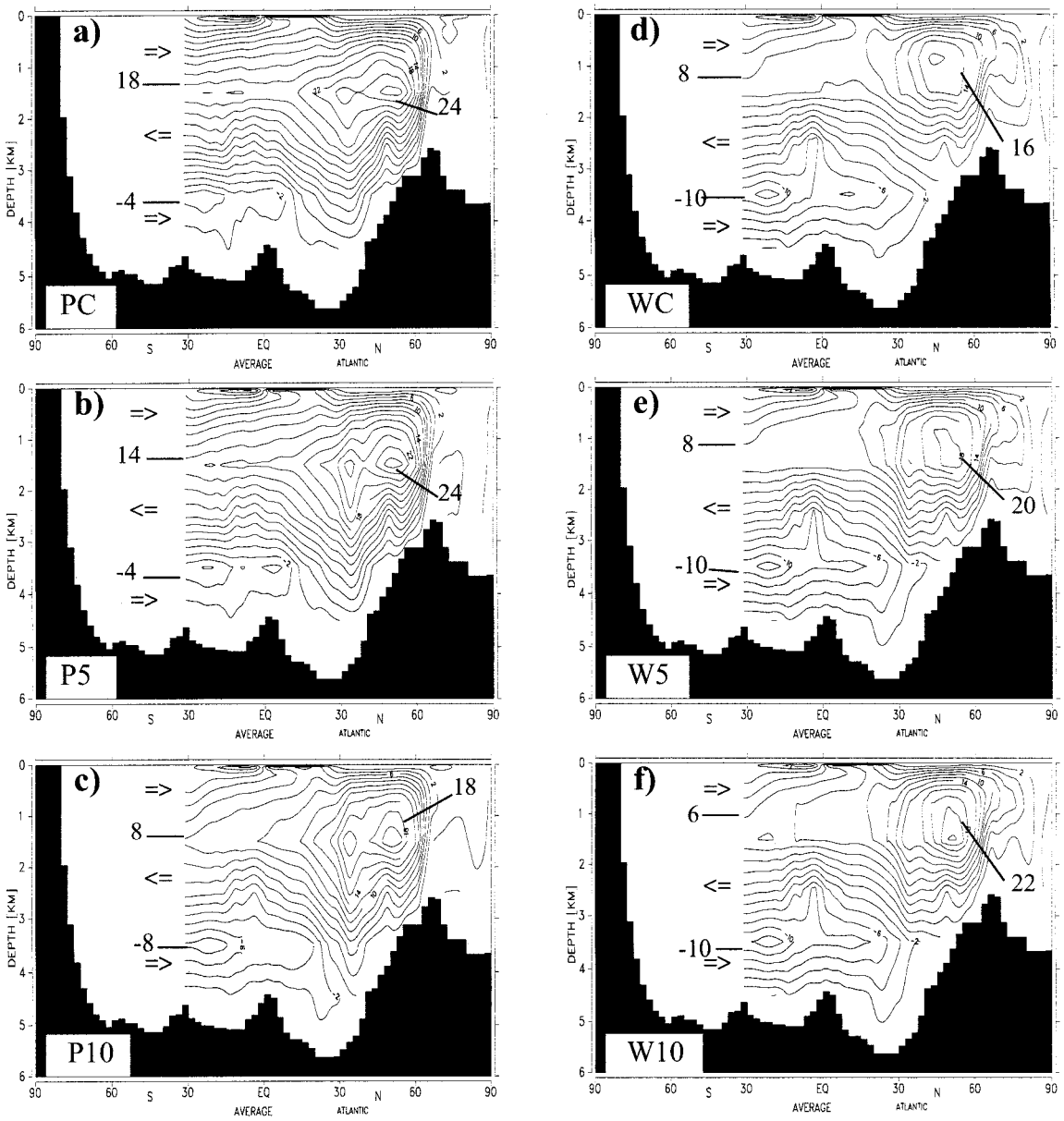

FIG. 8. Zonally integrated Atlantic meridional circulation for present climate (a) control (PC), (b) P5, and (c) P10 and for the warm ($2 \times CO_2$) climate (d) control (WC), (e) W5, and (f) W10. The simulations are defined in Fig. 4. The values are averaged over the last year of the simulations when stationary states were obtained. The values are in Sverdrups (Sv $\equiv 10^6$ m^3 s^{-1}). Contour interval is 2 Sv.

show that oscillations are more extensive for the present compared to the warm climate.

It is of interest to investigate if the drift and variability for the two climates are associated with different modes of the Atlantic thermohaline circulation. Figure 8 shows vertical cross sections of meridional volume transport for the Atlantic Ocean. The meridional circulation for PC (Fig. 8a) is characterized by an upper inflow (above 1500 m) at 30°S of about 18 Sv, an overturning in the North Atlantic of 24 Sv and a deep return flow concentrated between 1500 and 3500 m. In the lowermost layers there is a weak inflow (2–4 Sv at 30°S) of Antarctic Bottom Water (AABW) reaching approximately to the equator. The differences between PC and P1 are minor (not shown). The upper inflow (at 30°S) is reduced from 18 Sv for PC to 14 and 8 Sv for P5 and P10 respectively (Figs. 8b,c), and thus the coupling between the Atlantic and the Southern Ocean is reduced. The strength of the thermohaline overturning in the North Atlantic is 24 Sv for PC and P5 and 18 Sv for P10. The changes in the North Atlantic overturning are thus smaller than the changes in the South Atlantic upper

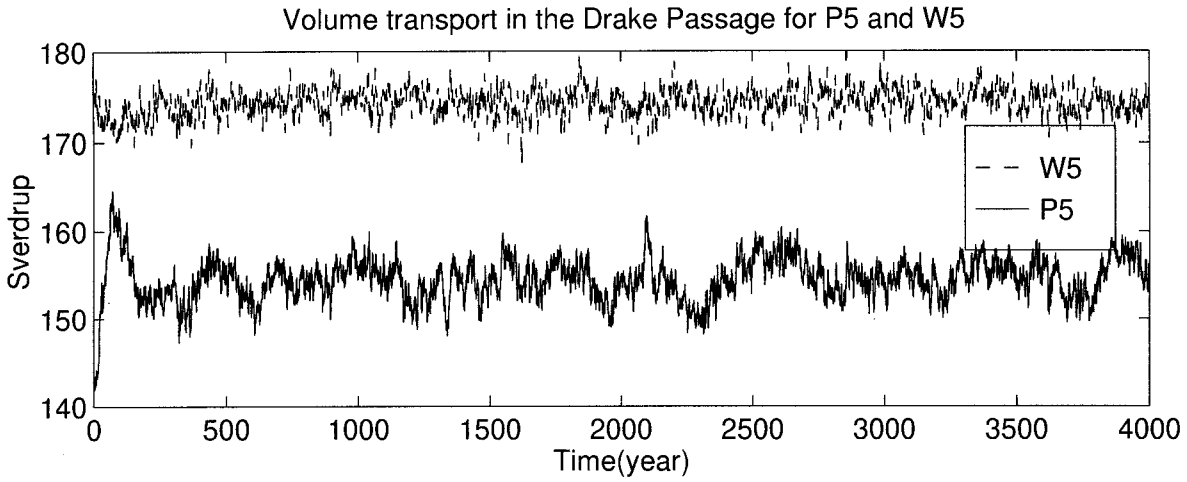

FIG. 9. Time series of the volume transport in Drake Passage for P5 and W5.

inflow. Another point is that the rate of AABW and upper-layer inflow into the Atlantic are oppositely correlated (e.g., cf. Figs. 8a and 8c), which Maier-Reimer et al. (1993) also found in simulations with different formulations of the boundary conditions for salt and heat.

The circulation for WC (Fig. 8d) is dominated by an upper inflow of 8 Sv at 30°S, a thermohaline overturning of about 16 Sv in the North Atlantic, and a deep inflow of AABW (about 10 Sv at 30°S) penetrating northward to 45°N. The circulation patterns for the simulations W1 (not shown), W5, and W10 (Figs. 8e,f) are similar. However, the North Atlantic overturning increases with increasing noise from 16 Sv for WC to 20 and 22 Sv for W5 and W10 respectively. In combination the results indicate that the meridional circulation in the Atlantic for the present climate approaches that of the warm climate as the noise increases.

The time series of the Drake Passage transport for P5 and W5 are shown in Fig. 9. Oscillations on secular timescales are more prominent for the present compared to the warm climate. The drift is minor for W5, whereas for P5 the time series indicates that the adjustment to the stochastic noise occurs within a few hundred years. After this time the oscillations occur about a relatively steady state.

The response to the white noise forcing was investigated by estimating power spectra of the volume transport in Drake Passage for selected simulations. We are mainly interested in variability on decadal and longer timescales. Therefore a maximum entrophy method (MEM) (Childers 1978) was preferred to the fast Fourier transform (FFT) method for the estimation of the power spectrum because of its advantage in the frequency resolution. Dependent on the chosen frequency interval, the MEM estimation can have a finer resolution, especially for low frequencies, than the FFT method. Figure 10 shows the estimated power spectra. The 99% confidence interval is calculated by using the fact that asymptotically the statistical properties of the MEM estimator are approximately equivalent to those of periodogram-based estimators (Haykin and Kesler 1979). The energy connected to the oscillation is generally somewhat higher for P1 compared to W1 (Fig. 10a), with the exception of the shortest periods where the differences are small. Note that the maximum peak is found at about 250 yr for both climates. Comparison of the power spectra for P5 and W5 (Fig. 10b) reveals significant differences on the secular timescales. On periods longer than 250 yr significantly more energy is accumulated for P5 than for W5. On decadal timescales the differences are negligible.

5. The box model

A box model is developed to illuminate some aspects of the role of the heat flux parameterization in the variability of the thermohaline circulation. A second objective is to illustrate how different buoyancy fluxes may affect the variability of the circulation.

The model has similarities to those used by, for example, Welander (1982), Lenderink and Haarsma (1994), and Pierce et al. (1995). However, the surface condition for temperature is different. Unlike the model in the last reference, the lower-layer temperature and salinity are fixed since here our primary interest is in how the surface layer is affected by different surface conditions. Pierce et al. (1995) used a pure restoring for the temperature boundary condition while we use a weighted function of restoring and flux, which mirrors the different types of the temperature boundary condition. The heat flux boundary parameterization used in our OGCM simulations (mix of a restoring term and a prescribed flux term) is then investigated versus using a pure restoring condition.

Another important difference between our box model

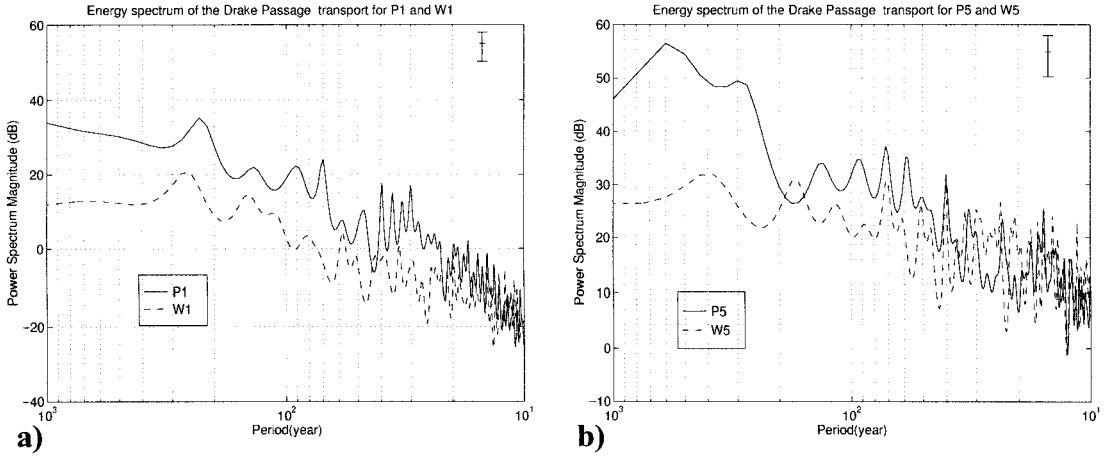

FIG. 10. Spectrum of the volume transport in Drake Passage (years 1000–4000) for the two climates (a) the spectrum for P1 and W1 and (b) the spectrum for P5 and W5. A maximum entropy method with 400 poles is used to calculate the power spectrum. The 99% confidence interval is indicated in the upper-right corner.

and that of Pierce et al. (1995) is that they used a constant mixing coefficient between the upper and lower layers. We will let the mixing coefficient vary with temperature and salinity. A schematic view of the model is shown in Fig. 11.

The temperature and salinity in the upper layer are determined by the surface heat and freshwater flux and the mixing with the lower layer. The model equations are

$$\frac{\partial T_1}{\partial t} = Q + K(T_2 - T_1) \tag{4}$$

$$\frac{\partial S_1}{\partial t} = -F + K(S_2 - S_1), \tag{5}$$

where subscript 1 and 2 refer to the upper and lower layer respectively, K is a mixing coefficient, Q is the heat flux condition at the surface, and $F \equiv \overline{S}F_{P-E}/h$ where h is the upper-layer thickness, $\overline{S}$ is a surface reference salinity, and F_{P-E} is the net freshwater flux. We let Q be a combination of both restoring and prescribed flux:

$$Q = r\frac{\kappa(T_a - T_1)}{h\rho_0 c_p} + (1 - r)\frac{H_f}{h\rho_0 c_p}, \tag{6}$$

where T_a is the air temperature, κ is the relaxation constant, ρ_0 is a reference density, c_p is the heat capacity of seawater, and H_f is the prescribed heat flux. The weight function r determines the different types of the heat flux boundary conditions; $r = 1$ is a pure restoring condition, $r = 0$ is an only flux condition, while $0 < r < 1$ is a mix of flux and a restoring. Here H_f is diagnosed from

$$H_f = \kappa(T_a - T_c), \tag{7}$$

where T_c is the upper-layer temperature from the spinup run.

Using Eqs. (6) and (7), the stationary solution of Eq. (4) is

$$T_1 = \frac{r\kappa T_c + H_f}{r\kappa + Kh\rho_0 c_p}. \tag{8}$$

The mixing coefficient K in the model depends on the stability of the water column and is a function of the density difference between upper and lower layers. Unlike Pierce et al. (1995), who used a constant K, we assume that it is a variable that depends on temperature and salinity. The only criterion is that K is the same in both the equations for temperature and salinity [Eqs. (4) and (5)]. Instead of solving the equations for T_1 and S_1, we then eliminate K and find T_1 as a function of S_1. Other box models have connected the upper-layer salinity and temperature by a linear or a simple nonlinear function of the equation of state. We will instead plot the solutions of T_1 and S_1 in a T–S diagram where the

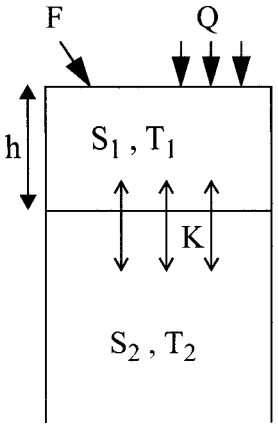

FIG. 11. Schematic view of the model. The two-layer model has constant temperature and salinity in the lower layer. The temperature and the salinity in the upper layer are balanced by atmospheric forcing and mixing with the lower layer.

TABLE 1. Parameters that are kept constant in Eq. (10).

T_a	T_c	T_2	S_2	α	β
−5°C	−1°C	1°C	34.7 psu	6×10^{-5} K^{-1}	8×10^{-4} psu^{-1}

full UNESCO-83 formula is used to determine the density.

The mixing coefficient in the stationary solution of Eq. (5) is

$$K = \frac{B_F}{\beta g h (S_2 - S_1)}, \tag{9}$$

where β is the salinity expansion coefficient and $B_F = \beta g \bar{S} F_{P-E}$ is the buoyancy flux due to net freshwater flux.

By combining Eqs. (8) and (9), the upper-layer temperature can be written

$$T_1 = T_c + (T_c - T_a)\frac{\gamma(T_2 - T_c) + R(S_2 - S_1)}{\gamma(T_c - T_a) - rR(S_2 - S_1)}, \tag{10}$$

where $\gamma = \alpha/\beta$ and α is the thermal expansion coefficient; R is the ratio $R = B_H/B_F$, where $B_H = \alpha g H_f/(\rho_0 c_p)$ is the buoyancy flux due to heat flux.

We consider the case of a cold and fresh upper layer relative to the lower layer, which is generally the case at high latitudes. Table 1 contains the values of parameters, which are kept constant in the model.

In Fig. 12 the solutions of Eq. (10) are shown for $R = 1$ with three choices of r (0, 0.4, 1). The location of the steady state (T_1, S_1) is along lines for constant r but depends on K and the heat and freshwater fluxes. The lower intersection of the three lines is the point that corresponds to the control run state for layer one (T_c, S_c). Here S_c can be calculated by setting $T_1 = T_c$ in Eq. (10). The point in the upper right corner represents the state for layer two (T_2, S_2). To illustrate the effect that the choice of r has in generating oscillations we assume an initial state (T_c, S_c). An anomaly in the freshwater forcing will alter S_1 [from Eq. (5)], which results in a change in T_1. Figure 12 shows that the density changes increase with increasing r. This implies that under pure restoring condition for temperature ($r = 1$) the likelihood for oscillations is larger than for the choice of a smaller r.

Based on simulations with the LSG model, Pierce et al. (1995) estimated R to average 1.1 south of 60°S for the present climate. They observed that oscillations did not occur when the net freshwater flux was roughly changed by more than ±30% corresponding to a range of R from 0.8 to 1.6. In Fig. 13 we show the stability of the solutions due to varying R (e.g., connected to the temperature dependency of α or altered heat or freshwater fluxes). The curves represent the solutions of Eq. (10) for three choices of R (0.8, 1.1, and 1.6). We use $r = 0.4$, which is similar to what we used in our simulations with the LSG model. The point in the upper-right corner represents the state for the lower layer (T_2, S_2). Now assume a perturbation in the freshwater flux that leads to a change in S_1. To find the equivalent change in T_1 recall that the solutions must be on the respective curves dependent on R. Figure 13 shows the response to such perturbation: for $R = 0.8$ the stratification will always be stable; for $R = 1.1$ stratification

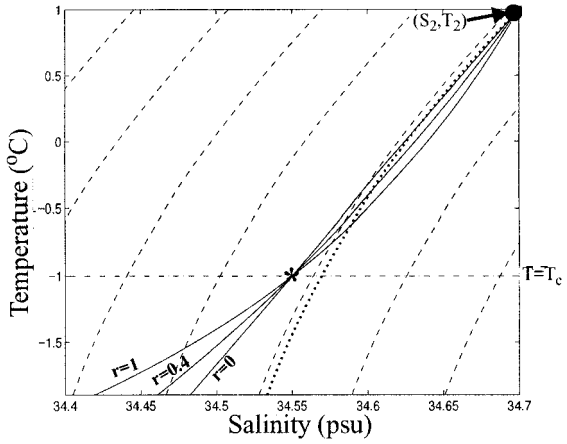

FIG. 12. Curves for T_1 and S_1 calculated from Eq. (10) with three different r. Different values of r represent different types of heat flux boundary condition: $r = 1$ is pure restoring, $r = 0$ is pure flux, while $r = 0.4$ is a mix of both restoring and flux. The dashed lines represent isopycnals where the UNESCO-83 formula is used to calculate the density. The dotted line is the isoline for $\rho(S_2, T_2)$. The asterisk is the control point (S_c, T_c) where the perturbation of the freshwater flux starts from. A salinity anomaly will give larger density anomaly for larger r since the solutions must be on the lines for constant r.

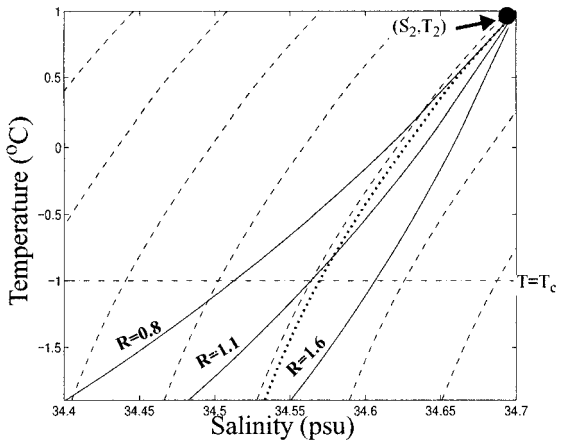

FIG. 13. Curves for T_1 and S_1 calculated from Eq. (10) with $r = 0.4$ with different values of R: 0.8, 1.1, and 1.6. The solution for $R = 0.8$ will always have a density lower than that from the lower layer, while $R = 1.6$ always has a larger density. The line for $R = 1.1$ is the only one that can have both convective and nonconvective periods.

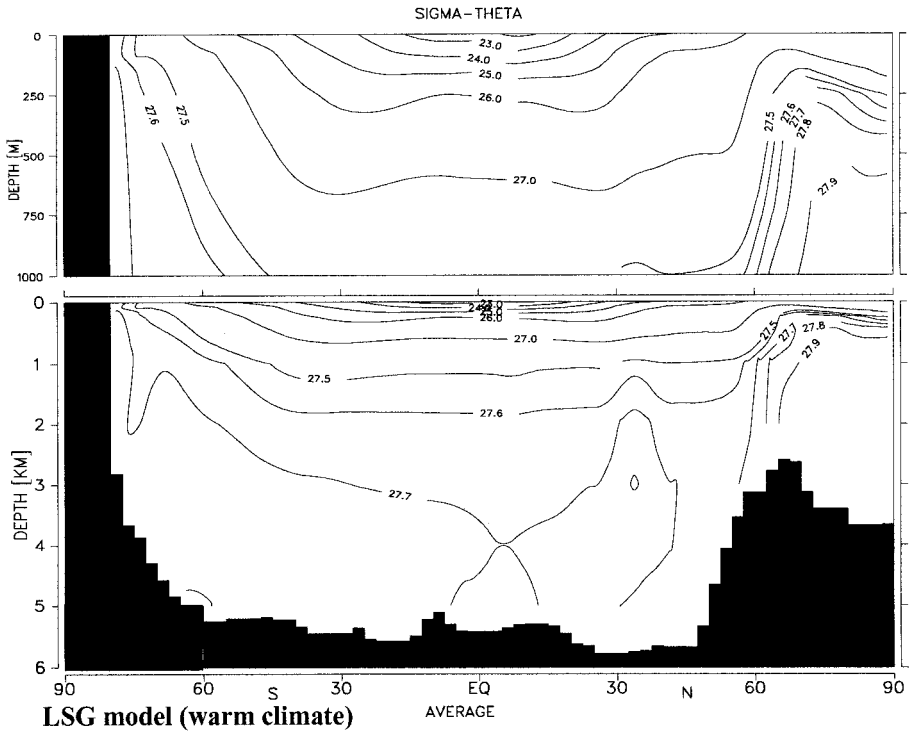

FIG. 14. Annual global zonal average of σ_θ from the control run of the LSG model for the warm climate.

can switch between stable and unstable, thus oscillations are possible whereas $R = 1.6$ represents an unstable state with continuous overturning.

These results are also consistent with the results from the box model by Lenderink and Haarsma (1994), where existence of both convective and nonconvective equilibria was possible when the ratio between surface freshwater flux and restoring temperature condition was bounded. Their ratio was modified a little compared to our ratio because they included horizontal advection and used a linear equation of state.

6. Discussion

The discussion is limited to processes at high latitude where the ocean generally loses heat to the atmosphere but gains freshwater. In the LSG model, thermohaline oscillations are generated mainly in the Southern Ocean. The mechanism driving these oscillations is similar as described in Pierce et al. (1995) and a brief summary of this is given in chapter 1. We will discuss various mechanisms that act to modify these oscillations.

a. Static stability for present and warm climate in the model

A central question is to what extent the larger variability found for the present compared to the warm climate is due to different static stability for the two climates. The static stability for the warmer climate would, for example, be larger if the surface ocean has warmed more than the deep ocean. Comparing the zonally averaged potential density fields for the present and the warm climate (Figs. 3b and 14) shows relatively minor differences. At low latitudes the vertical density gradients are slightly larger for the warm compared to the present climate, whereas in the Southern Ocean the static stability of the present climate exceeds that for the warm climate. The variability observed in our simulations is mainly due to convective variability occurring at high latitudes. Hence, it is not likely that the relatively minor increased static stability at low latitudes for the warm climate is the cause of the reduced variability.

b. The role of the buoyancy flux

A key result of the simulations is that, using similar stochastic freshwater forcing for both climates, the spectra for the LSG model on secular timescale shows higher energy for the present compared to the warm climate. This result could be related to the nonlinear terms in the equation of state, which modify the buoyancy forcing differently for the two climates. The ratio R (defined in §5) depends among other things on the expansion coefficients for temperature and salinity. The expansion coefficients α and β are, respectively, strongly and weakly dependent on temperature (Fig. 15). The buoyancy forcing due to the heat flux becomes relatively

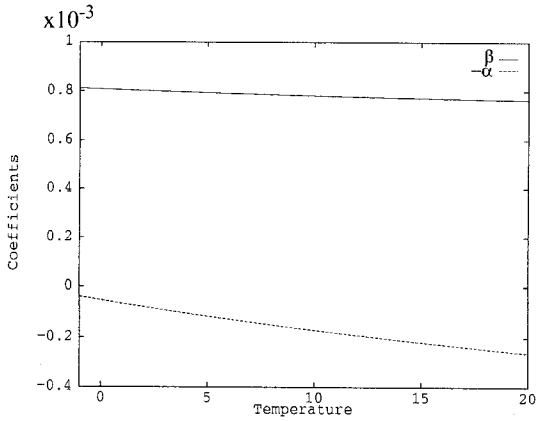

FIG. 15. The temperature dependence of the expansion coefficients for respectively temperature ($-\alpha$) and salinity (β).

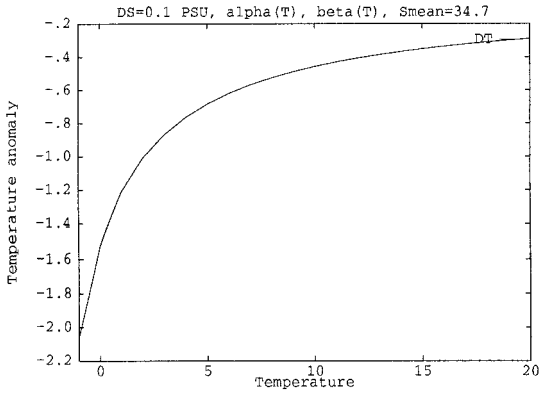

FIG. 16. The equivalent temperature anomaly ($\Delta T = -\beta \Delta S/\alpha$) needed to balance a salinity anomaly of -0.1 psu as a function of temperature. The reference salinity $\overline{S} = 34.7$ psu.

more dominant for density variation at high temperatures. A temperature increase of 4°C, which is the mean difference between the present and warm climate, from 0° to 4°C, increases α by 94%. This would increase R from 1.1, corresponding to the present climate, to 2.1 for the warm climate assuming similar heat and freshwater fluxes.

Pierce et al. (1995) investigated secular oscillations originating in the Southern Ocean in terms of the heat flux and freshwater flux. They concluded that a necessary condition for such oscillations is that R is close to 1. In this case the nonlinear effects in the equation of state could potentially switch the leading term, with respect to buoyancy changes, from the freshwater flux to the heat flux and vice versa. Hence both convective and nonconvective periods are possible. The results from the box model (Fig. 13) are consistent with the results from Pierce et al. (1995). Due to its simplicity, the results based on the box model cannot be regarded as definitive, but they illustrate mechanisms that are potentially important for OGCMs.

Based on the diagnostic fluxes we estimated a mean ratio R (south of 60°S) of 2.8 for the warm climate (compared to 1.1 for the present climate). Results from the box model show that this value is far beyond the limit for generating oscillations. This is also in accordance with the smaller variability for the warm climate relative to the present climate in the LSG simulations. For the warm climate the buoyancy flux is dominated by the heat flux. Convection occurs ''continuously'' and a larger noise is required to generate secular oscillations.

In the present-day circulation, the two components of the buoyancy flux tend to cancel each other out. Surface anomalies occur most frequently in pairs of either fresh and cold or saline and warm. The temperature anomaly needed to compensate the altered buoyancy due to a salinity anomaly decreases with increasing temperature (Fig. 16). This may explain the larger variability for the present compared to the warm climate found in our simulations.

c. The role of the heat flux boundary condition

Results from the simulations with white noise of standard deviation of 80 mm/month added to the freshwater flux (P1 and W1) showed no significant drift or variability in the volume transport through Drake Passage for either climate (see Fig. 7). With a noise of standard deviation of 16 mm/month added to the freshwater flux, Mikolajewicz and Maier-Reimer (1990) got large secular oscillations in the Drake Passage transport with a peak to peak amplitude of about 90 Sv. Based on the larger noise used in our simulations we could expect significant variability and drift. However, for the heat flux boundary condition they used a pure restoring condition with a relaxation constant of 40 W m^{-2} K^{-1}, while we applied the mix of prescribed flux and weaker restoring (relaxation constant of 16 W m^{-2} K^{-1}) suggested by Mikolajewicz and Maier-Reimer (1994). With this boundary condition a repeated simulation of Mikolajewicz and Maier-Reimer (1990) resulted in no secular oscillation in the Drake Passage transport and an eightfold increase of the noise (standard deviations of the noise is 128 mm/month) was necessary to obtain significant secular oscillations (Mikolajewicz and Maier-Reimer 1994).

Results from the box model (§5) also illustrate the impact of the heat flux boundary condition on the variability of the thermohaline circulation. A salinity anomaly at the surface (e.g., noise added to the freshwater flux) gives a larger density change when a pure restoring condition is used compared to the mixed condition (similar to that used in our simulations). As changes in the density influence the thermohaline circulation, this is consistent with the discussed results from OGCM simulations (e.g., Mikolajewicz and Maier-Reimer 1990, 1994).

The Drake Passage transport increases with increasing noise for the present climate (by 3 Sv for P1, 14 Sv for P5, and 30 Sv for Pl0). Power (1995) found similar results when using a pure restoring heat flux

condition in simulations with the GFDL model. He also noted that when applying weaker restoring in the heat flux condition, larger noise was required to obtain similar change in the transport. This corresponds to the role discussed above of the heat flux boundary condition (pure restoring vs mix of weaker restoring and flux). For the warm climate we observed no similar trend (0.5 Sv for W1, 2 Sv for W5, and 10 Sv for W10) compared to that for the present climate. The prescribed heat fluxes used in the boundary condition for the warm climate has larger values around Antarctica (e.g., due to reduced extent of sea ice) compared to that for the present climate. This difference in the boundary condition between the two climates could play an important role in the variability of the ACC.

7. Conclusions

The variability of the solutions, measured as the volume transport through Drake Passage, for the present climate exceeds that of the warm climate. For increasing levels of stochastic freshwater forcing, the Drake Passage transport and the Atlantic meridional circulation for the present climate approaches that of the warm climate.

The bouyancy forcing for the present climate has a higher potential to trigger secular thermohaline oscillations compared to that for the warm climate. In the present climate the two buoyancy fluxes due to heat and freshwater are of similar magnitudes but with opposite signs, so that switches between convective and nonconvective periods at secular timescales are possible. In the case of the warm climate, the buoyancy flux due to heat dominates over the buoyancy flux due to freshwater and oscillations at secular timescales are less probable. Another explanation for the different rates of variability could be the stronger coupling between the Atlantic and the Southern Ocean for the present relative to the warm climate.

Comparison with previous work suggests that the boundary condition for sea surface temperature, mixture of heat flux, and temperature restoring is much less likely to generate switches between various circulation modes than using a pure temperature restoring condition.

Acknowledgments. We thank Knut Barthel and Peter M. Haugan for useful discussions and constructive comments on the text. We would also thank Ernst Maier-Reimer and Uwe Mikolajewicz at the Max-Planck-Institut für Metereologie in Hamburg for providing us with the model and the data fields. The two anonymous reviewers also deserve thanks for constructive critiques and good suggestions that helped to improve the manuscript. This work has received support from The Research Council of Norway through Project No. 101533/720 and a grant of computing time (Program for Supercomputing).

REFERENCES

Barnett, T. P., M. Chu, R. Wilde, and U. Mikolajewicz, 1993: Low frequency ocean variability induced by stochastic forcing of various colours. *Proc. Fourth Conf. on Global Climate Studies*, Anaheim, CA, Amer. Meteor. Soc., 29–30.

Baumgartner, A., and E. Reichel, 1975: *The World Water Balance.* Elsevier, 179 pp.

Boyle, E. A., and L. Keigwin, 1987: North Atlantic thermohaline circulation during the past 20,000 years linked to high-latitude surface temperatures. *Nature,* **330,** 35–40.

Broecker, W. S., 1991: The great ocean conveyer. *Oceanography,* **4,** 79–89.

Bryan, F., 1986: High-latitude salinity effects and interhemispheric thermohaline circulations. *Nature,* **323,** 301–304.

Childers, D. G., 1978: *Modern Spectrum Analysis.* IEEE Press, 334 pp.

Frankignoul, C., and K. Hasselmann, 1977: Stochastic climate models. Part II: Application to sea-surface temperature anomalies and thermocline variability. *Tellus,* **29,** 289–305.

Hansen, J., A. Lacis, D. Rind, G. Russell, P. Stone, I. Fung, R. Ruedy, and J. Lerner, 1984: Climate sensitivity: Analysis of feedback mechanisms. *Climate Processes and Climate Sensitivity,* J. Hansen and T. Takahashi, Eds., Amer. Geophys. Union, 130–163.

Hasselmann, K., 1976: Stochastic climate models. Part I: Theory. *Tellus,* **28,** 473–485.

——, 1982: An ocean model for climate variability studies. *Progress in Oceanography,* Vol. 11, Pergamon, 69–92.

Haykin, S., and S. Kesler, 1979: Prediction-error filtering and maximum-entropy spectral estimation. *Nonlinear Methods of Spectral Analysis,* Chapter 2. S. Haykin, Ed., Springer-Verlag, 9–72.

Hellermann, S., and M., Rosenstein, 1983: Normal monthly windstress over the World Ocean with error estimates. *J. Phys. Oceanogr.,* **13,** 1093–1104.

Keigwin, L. D., G. A. Jones, S. J. Lehman, and E. A. Boyle, 1991: Deglacial melt-water discharge, North Atlantic deep circulation, and abrupt climate change. *J. Geophys. Res.,* **96**(C9), 16 811–16 826.

Lenderink, G., and R. J. Haarsma, 1994: Variability and multiple equilibria of the thermohaline circulation associated with deep-water formation. *J. Phys. Oceanogr.,* **24,** 1480–1493.

Levitus, S., 1982: *Climatological Atlas of the World Ocean.* NOAA Prof. Paper No. 13, U.S. Dept. of Commerce, 173 pp.

——, and T. Boyer, 1994: *World Ocean Atlas, 1994.* Vol. 4: *Temperature.* NOAA, U.S. Dept. of Commerce, 117 pp.

——, R. Burgett, and T. Boyer, 1994: *World Ocean Atlas, 1994.* Vol. 3: *Salinity.* NOAA, U.S. Dept. of Commerce, 99 pp.

Maier-Reimer, E., and U. Mikolajewicz, 1989: Experiments with an OGCM on the cause of the Younger Dryas. *Oceanography,* UNAM Press, 87–100.

——, ——, and K. Hasselmann, 1993: Mean circulation of the Hamburg LSG OGCM and its sensitivity to the thermohaline surface forcing. *J. Phys. Oceanogr.,* **23,** 731–757.

Marotzke, J., 1989: Instability and multiple steady states of the thermohaline circulation. *Oceanic Circulation Models: Combining Data and Dynamics,* D. L. T. Anderson and J. Willebrand, Eds., NATO ASI Series, Kluwer, 501–511.

——, P. Welander, and J. Willebrand, 1988: Instability and multiple steady states in a meridional-plane model of the thermohaline circulation. *Tellus,* **40A,** 162–172.

Mikolajewicz, U., and E. Maier-Reimer, 1990: Internal secular variability in an ocean general circulation model. *Climate Dyn.,* **4,** 145–156.

——, and ——, 1994: ''Mixed boundary conditions'' in an OGCM and their influence on the stability of the model's conveyor belt. *J. Geophys. Res.,* **99**(C11), 22 623–22 644.

Mork, K. A., and Ø. Skagseth, 1996: Modelling the ocean response to secular surface temperature transitions. *Climate Dyn.,* **12,** 653–666.

Mysak, L. A., T. F. Stocker, and F. Huang, 1993: Century-scale vari-

ability in a randomly forced, two-dimensional thermohaline ocean circulation model. *Climate Dyn.,* **8,** 104–116.

Pierce, D. W., T. P. Barnett, and U. Mikolajewicz, 1995: Competing roles of heat and freshwater flux in forcing thermohaline oscillations. *J. Phys. Oceanogr.,* **25,** 2046–2064.

Power, S. B., 1995: Climate drift in global ocean general circulation model. *J. Phys. Oceanogr.,* **25,** 1025–1036.

——, and R. Kleeman, 1994: Surface heat flux parameterisation and the response of ocean general circulation models to high latitude freshening. *Tellus,* **46A,** 86–95.

Rahmstorf, S., and J. Willebrand, 1995: The role of temperature feedback in stabilizing the thermohaline circulation. *J. Phys. Oceanogr.,* **25,** 787–805.

Schlesinger, M. E., and Z. C. Zhao, 1989: Seasonal climatic changes induced by doubled CO_2 as simulated by the OSU Atmospheric GCM/Mixed-Layer Ocean Model. *J. Climate,* **2,** 459–495.

Seager, R., Y. Kushnir, and M. A. Cane, 1995: On heat flux boundary conditions for ocean models. *J. Phys. Oceanogr.,* **25,** 3219–3230.

Stommel, H., 1961: Themohaline convection with two stable regimes of flow. *Tellus,* **13,** 224–230.

Taylor, K. C., G. W. Lamoray, G. A. Doyle, R. B. Alley, P. M. Grootes, P. A. Mayewski, J. W. C. White, and L. K. Barlow, 1993: The ''flickering switch'' of late Pleistocene climate change. *Nature,* **361,** 432–435.

Toggweiler, J. R., and B. Samuels, 1993: Is the magnitude of the deep outflow from the Atlantic Ocean actually governed by Southern Hemisphere winds? *The Global Carbon Cycle.* M. Heimann, Ed., NATO ASI Series, Springer-Verlag, 303–331.

Weaver, A. J., J. Marotzke, P. F. Cummins, and E. S. Sarachik, 1993: Stability and variability of the thermohaline circulation. *J. Phys. Oceanogr.,* **23,** 39–60.

Welander, P., 1982: A simple heat salt oscillator. *Dyn. Atmos. Oceans,* **6,** 233–242.

——, 1986: Thermohaline effects in the ocean circulation and related simpler models. *Large-Scale Transport Processes in Oceans and Atmosphere,* J. Willebrand and D. L. T. Anderson, Eds., D. Reidel, 163–200.

Wetherald, R. Y., and S. Manabe, 1986: An investigation of cloud cover change in response to thermal forcing. *Climate Change,* **8,** 5–23.

Wilson, C. A., and J. F. B. Mitchell, 1987: A double CO_2 climate sensitivity experiment with a global climate model including a simple ocean. *J. Geophys. Res.,* **92,** 3315–3343.

Winton, M., and E. S. Sarachik, 1993: Thermohaline oscillations induced by strong steady salinity forcing of ocean general circulation models. *J. Phys. Oceanogr.,* **23,** 1389–1410.

Woodruff, S. D., R. J. Slutz, R. L. Jenne, and P. M. Steurer, 1987: A comprehensive ocean–atmosphere dataset. *Bull. Amer. Meteor. Soc.,* **68,** 1239–1250.